Structural Engineering and Mechanics, Vol. 42, No. 2 (2012) 269-289
DOI: http://dx.doi.org/10.12989/sem.2012.42.2.269

Dynamic analysis of semi-rigidly connected and partially embedded piles via the method of reverberation-ray matrix

Wei Yan*[1] and W.Q. Chen[2]

[1]*Faculty of Architectural, Civil Engineering and Environment, Ningbo University, Ningbo 315211, P.R. China*
[2]*Department of Engineering Mechanics, Zhejiang University, Yuquan Campus, Hangzhou 310027, P.R. China*

(Received April 25, 2011, Revised February 26, 2012, Accepted February 29, 2012)

Abstract. Free vibration and dynamic responses of piles semi-rigidly connected with the superstructures are investigated. Timoshenko beam theory is employed to characterize the pile partially embedded in a two-parameter elastic foundation. The formulations for the method of reverberation-ray matrix (MRRM) are then derived to investigate the dynamics of the pile with surface cracks, which are modeled as massless rotational springs. Comparison with existent numerical and experimental results indicates the proposed method is very effective and accurate for dynamic analysis, especially in the high frequency range. Finally, the effects of some physical parameters on the natural frequencies, frequency responses and transient responses of the piles are studied.

Keywords: pile; semi-rigid; timoshenko beam theory; reverberation-ray matrix; dynamic analysis

1. Introduction

Piles are widely used in the fields of civil engineering, ocean engineering and the like when the strength of soil base is insufficient to support the load from the superstructures. Although many approaches have been developed for static pile foundation design in past decades, due to various dynamic loads such as seismic waves, vibration responses of piles should be taken into account in the design of pile foundation to satisfy the practical requirements (Lu *et al.* 2006). On the other hand, many hazardous factors such as a seismic load may generate dramatic damages to pile foundations (Lu *et al.* 2006) and thus some robust structural health monitoring techniques (Lee and Shin 2002), including the impedance-based method (Bamnios 2002), should be implemented to detect the defects in piles. Consequently, the understanding of dynamic behavior of piles is very crucial in the field of engineering.

It is commonly assumed that the upper ends of the piles are simply supported (Catal 2002) or fully rigidly connected with the superstructures such as offshore platforms, bridge beams etc (Arboleda-Monsalve *et al*. 2008). However, due to the cross-section and material properties of the piles, these connections are neither fully rigid nor completely flexible and a semi-rigid connection

*Corresponding author, Ph.D., E-mail: yanwei4467@sohu.com

model denoted by the bending stiffness indices is considered to be more appropriate to depict the behavior of the joints between the piles and the superstructures (Catal 2006). The dynamic behavior of the beams or piles with semi-rigid connections has been investigated by many researchers (Sekulovic *et al.* 2002, Catal 2006, Arboleda-Monsalve *et al.* 2008, Faella *et al.* 2008, Yesilce and Catal 2008a, b, c) in the past several years. All these researches show that the connection semi-rigidity plays an important role in the global behavior of structures. Moreover, a crack appearing in a pile or a beam can be model as a rotational spring, which can also be associated with a semi-rigid connection (Bamnios 2002, Lin 2004).

The classical dynamic analysis techniques such as finite element method (FEM) (Faella *et al.* 2008), the method of dynamic stiffness matrix (Sekulovic *et al.* 2002, Arboleda-Monsalve *et al.* 2008) and the transfer matrix method (Catal 2006) have been employed to investigate structures with semi-rigid joints. However, FEM is not only particularly hard and expensive where extraordinary many elements and nodes need to be included but also yields in doubtful numerical results, especially at high frequencies (Lee and Shin 2002). The transfer matrix method is very powerful to analyze a structure consisting of many members because the number of resultant simultaneous equations can be greatly reduced (Nagem and Williams 1989). However, significant numerical difficulty at high frequency limits its application if computation is completely executed on a computer (Pestel and Leckie 1963, Yan *et al.* 2007a, b). This numerical difficulty appears simply because, for a large wave number or long length of the structural member contained in the transfer matrix, the hyperbolic function gives an extremely large number compared to that of the sine function, and the latter may be completely submerged because of the finite digits retained in the computation. The method of dynamic stiffness matrix can provide more accurate dynamic solutions than FEM (Lee and Shin 2002), but it will also suffer from numerical instability in the high frequency range as TMM does. Although structural analysis in the field of conventional engineering only addresses low frequency behavior, it is reported that recent advances in fracture mechanics and crack diagnosis require knowledge of the effect on the high frequency response of a micro-crack before a catastrophic macro-crack is evolved (Bhalla and Soh 2004, Morikawa *et al.* 2005, Yan *et al.* 2008). Note that the method of reverberation-ray matrix (MRRM) (Pao *et al.* 2007, Pao and Chen 2009), which is based on the concept of elastic wave propagation, has shown its great superiority on high-frequency response analysis in our previous works (Yan *et al.* 2007a, 2007b, Yan *et al.* 2008) .

This paper investigates the free vibration, frequency responses and transient responses of a pile partially embedded in soil (Catal and Catal 2006, Rajasekaran 2008). The pile is semi-rigidly connected with the superstructure and the single-sided open cracks initiating in the pile are modeled as rotational springs (Lin 2004). The coupling effects of translational and rotational lumped masses as well as the applied axial force at the upper end are considered. The pile, which is usually modeled as a beam (Catal 2002, 2006, Allotey and EI Naggar 2008), is partially embedded in a two-parameter elastic foundation (Celep *et al.* 2011) with generalized end conditions. The formulations for the method of reverberation-ray matrix (MRRM) (Pao *et al.* 2007, Pao and Chen 2009) are given to investigate the dynamics of the pile with flexible joints. It should be noted that, the beam model is very simple to simulate the pile, but it serves as a good example to illustrate our idea of investigating the dynamics for other types of basic structures such as trusses and thin-walled structures by MRRM. Both the free vibration and frequency responses (using mechanical impedance data) can directly be evaluated from MRRM to describe the dynamics of the piles. Then, the transient responses are determined through the application of inverse Fourier transforms.

2. Governing equations and general solutions

A pile whose upper end D is semi-rigidly connected against rotation is partially embedded in soil as shown in Fig. 1. It is assumed that a lumped mass m is attached at the extreme D with rotational moment of inertia J. A constant force N is loaded axially at the upper end of the pile along its centroidal axis x. A two-parameter elastic foundation model, in which both the ballast modulus k_s and the transverse modulus k_G are taken into account, is adopted in the paper. For a general pile segment embedded in the soil, we have the following relations based on the Timoshenko beam theory (Arboleda-Monsalve *et al.* 2008)

$$\frac{\partial M}{\partial x} - Q - \rho I \frac{\partial^2 \phi}{\partial t^2} + N\frac{\partial v}{\partial x} = 0, \quad M = EI\frac{\partial \phi}{\partial x}, \quad \frac{\partial Q}{\partial x} + \rho A \frac{\partial^2 v}{\partial t^2} + k_s v - k_G \frac{\partial^2 v}{\partial x^2} = 0 \tag{1}$$

The applied axial force N induces a shear component equal to $N\sin\phi \doteq N\phi$ according to the "modified shear approach" (Timoshenko and Gere 1961). Thus, the shear force equation becomes

$$Q = \kappa AG\left(\phi - \frac{\partial v}{\partial x}\right) + N\phi \tag{2}$$

Letting $\phi(x,t) = \bar{\phi}(x)e^{i\omega t}$ and $v(x,t) = \bar{v}(x)e^{i\omega t}$ by the method of separation of variables yields the following differential equations

$$(\kappa AG + N)\frac{\partial \bar{\phi}}{\partial x} - (\kappa AG + k_G)\frac{\partial^2 v}{\partial x^2} + (k_s - \rho A\omega^2)\bar{v} = 0 \tag{3}$$

$$EI\frac{\partial^2 \bar{\phi}}{\partial x^2} - (\kappa AG + N - \rho I\omega^2)\bar{\phi} + (\kappa AG + N)\frac{\partial v}{\partial x} = 0 \tag{4}$$

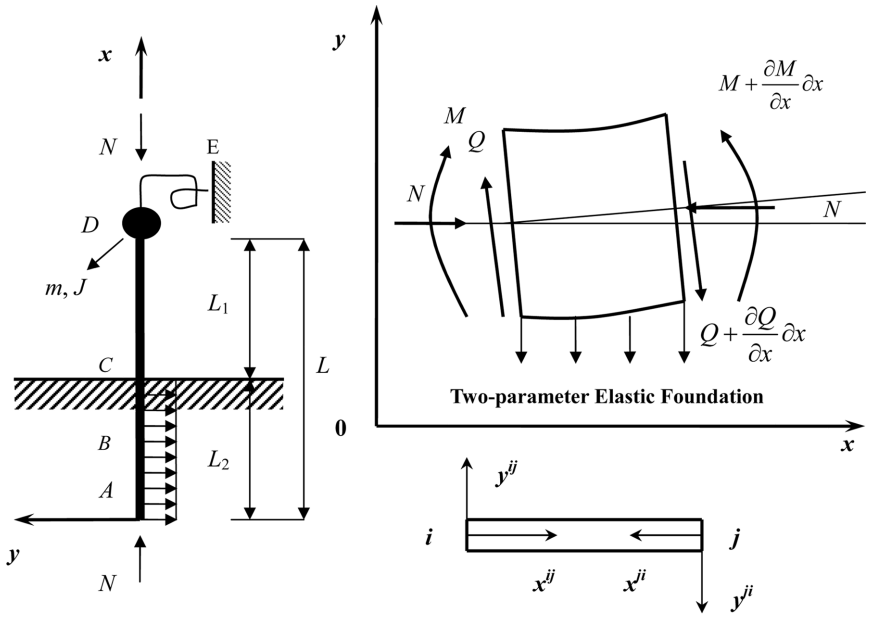

Fig. 1 A partially embedded pile with a semi-rigid connection and local coordinates

Eq. (3) can be rewritten as

$$\frac{\partial \overline{\phi}}{\partial x} = \frac{\kappa AG + k_G}{\kappa AG + N}\frac{\partial^2 \overline{v}}{\partial x^2} + \frac{\rho A\omega^2 - k_s}{\kappa AG + N}\overline{v} \tag{5}$$

Substituting Eq. (5) into Eq. (4) yields

$$\frac{\partial^4 \overline{v}}{\partial x^4} + \lambda_1 \frac{\partial^2 \overline{v}}{\partial x^2} + \lambda_2 \overline{v} = 0 \tag{6}$$

where

$$\lambda_1 = \frac{EI(\rho A\omega^2 - k_s) + \rho I\omega^2(\kappa AG + k_G) + (\kappa AG + N)(N - k_G)}{EI(\kappa AG + k_G)}$$

$$\lambda_2 = \frac{(k_s - \rho A\omega^2)(\kappa AG + N - \rho I\omega^2)}{EI(\kappa AG + k_G)} \tag{7}$$

The homogeneous solution of Eq. (6) is

$$\overline{v} = a_1 e^{\beta_1 x} + a_2 e^{\beta_2 x} + d_1 e^{-\beta_1 x} + d_2 e^{-\beta_2 x} \tag{8}$$

where

$$\beta_1 = \sqrt{\frac{\lambda_1 + \sqrt{\lambda_1^2 - 4\lambda_2}}{2}} \cdot i, \quad \beta_2 = \sqrt{\frac{-\lambda_1 + \sqrt{\lambda_1^2 - 4\lambda_2}}{2}} \tag{9}$$

Similarly, we have

$$\phi = (a_1\gamma_1 e^{\beta_1 x} + a_2\gamma_2 e^{\beta_2 x} - d_1\gamma_1 e^{-\beta_1 x} - d_2\gamma_2 e^{-\beta_2 x})e^{i\omega t} \tag{10}$$

where

$$\gamma_j = \frac{(\kappa AG + k_G)\beta_j^2 + \rho A\omega^2 - k_s}{(\kappa AG + N)\beta_j}, \quad (j = 1, 2) \tag{11}$$

The analytical expressions of v and ϕ for the pile element above the soil can also be derived in a similar way by simply setting $k_s = 0$ and $k_G = 0$ in Eq. (1).

3. Dynamic analysis based on MRRM

Having obtained pile deflection and rotation in Eqs. (8) and (10), the bending moment and shear force can be readily obtained according to Eqs. (1) and (2), respectively. At an arbitrary joint of the pile, force equilibrium and motion compatibility must be satisfied. For the cracked pile, four typical joints A (bottom end of the pile, at $x = 0$), B (crack position), C (ground surface, at $x = L_2$) and D (upper end of the pile, at $x = L$) should be considered. At joint C, we have the following continuity conditions

$$v^{CB} + v^{CD} = 0, \quad \phi^{CB} = \phi^{CD}, \quad M^{CB} + M^{CD} = 0, \quad Q^{CB} = Q^{CD}, \quad \text{at} \quad x^{CB} = x^{CD} = 0 \tag{12}$$

This equation immediately leads to the following relation

$$\mathbf{d}^C = \mathbf{S}^C \mathbf{a}^C \tag{13}$$

where $\mathbf{d}^C = [d_1^{CB}, d_2^{CB}, d_1^{CD}, d_2^{CD}]^T$ and $\mathbf{a}^C = [a_1^{CB}, a_2^{CB}, a_1^{CD}, a_2^{CD}]^T$ are called the departing wave vector and the arriving wave vector at joint C of order 4×1 (Pao *et al.* 2007, Pao and Chen 2009), respectively, and

$$\mathbf{S}^C = \begin{bmatrix} -1 & -1 & -1 & -1 \\ \gamma_1^{CB} & \gamma_2^{CB} & -\gamma_1^{CD} & -\gamma_1^{CD} \\ -(EI\gamma_1\beta_1)^{CB} & -(EI\gamma_2\beta_2)^{CB} & -(EI\gamma_1\beta_1)^{CD} & -(EI\gamma_2\beta_2)^{CD} \\ \eta_1^{CB} & \eta_2^{CB} & -\eta_1^{CD} & -\eta_2^{CD} \end{bmatrix}^{-1} \times \begin{bmatrix} 1 & 1 & 1 & 1 \\ \gamma_1^{CB} & \gamma_2^{CB} & -\gamma_1^{CD} & -\gamma_1^{CD} \\ (EI\gamma_1\beta_1)^{CB} & (EI\gamma_2\beta_2)^{CB} & (EI\gamma_1\beta_1)^{CD} & (EI\gamma_2\beta_2)^{CD} \\ \eta_1^{CB} & \eta_2^{CB} & -\eta_1^{CD} & -\eta_2^{CD} \end{bmatrix} \tag{14}$$

is called the local scattering matrix at joint C (Pao *et al.* 2007, Pao and Chen 2009) with rank four, where

$$\eta_j = \kappa AG(\gamma_j - \beta_j) + N\gamma_j, \qquad (j = 1, 2) \tag{15}$$

Eq. (13) establishes a scattering relation between various waves (traveling and standing waves) at node C.

At joint B (crack position), the compatibility conditions enforce continuities of deflection, bending moment and shear force across the crack. Meanwhile, beam slope discontinuity exists across the crack. The following relations (Lin 2004) can then be obtained

$$v^{BA} + v^{BC} = 0, \quad M^{BA} + M^{BC} = 0, \quad Q^{BC} = Q^{BA}, \quad \left(\frac{\partial v}{\partial x}\right)^{BC} - \left(\frac{\partial v}{\partial x}\right)^{BA} = \theta L \left(\frac{\partial \phi}{\partial x}\right)^{BC},$$

$$\text{at} \quad x^{BA} = x^{BC} = 0 \tag{16}$$

For single-sided open cracks, we have (Lin 2004)

$$\theta = 6\pi\gamma^2 f_J(\gamma)\left(\frac{h}{L}\right), \quad \gamma = \frac{c}{h}$$

$$f_J(\gamma) = 0.6384 - 1.035\gamma + 3.7201\gamma^2 - 5.1773\gamma^3 + 7.553\gamma^5 - 7.332\gamma^5 + 2.4909\gamma^6 \tag{17}$$

Substituting Eq. (17) into Eq. (16), the following relations in a matrix form are obtained

$$\mathbf{d}^B = \mathbf{S}^B \mathbf{a}^B \tag{18}$$

in which $\mathbf{d}^B = [d_1^{BA}, d_2^{BA}, d_1^{BC}, d_2^{BC}]^T$, $\mathbf{a}^B = [a_1^{BA}, a_2^{BA}, a_1^{BC}, a_2^{BC}]^T$, and $\mathbf{S}^B$ is the local scattering matrix of order 4×4 at joint B and can be derived from Eq. (16).

At two ends of the pile, the boundary conditions instead of continuity conditions must be imposed. The scattering matrices at the two ends, $\mathbf{S}^A$ and $\mathbf{S}^D$, thus have different forms and the order is reduced to 2×2. For illustration, we consider the free end (Catal 2006) at $x = 0$ (end A). To satisfy $Q = M = 0$, the following relation can be obtained from Eqs. (1) and (2)

$$\begin{Bmatrix} d_1^{AB} \\ d_2^{AB} \end{Bmatrix} = \begin{bmatrix} -(\gamma_1\beta_1)^{AB} & -(\gamma_2\beta_2)^{AB} \\ \eta_1^{AB} & \eta_2^{AB} \end{bmatrix}^{-1} \begin{bmatrix} (\gamma_1\beta_1)^{AB} & (\gamma_2\beta_2)^{AB} \\ \eta_1^{AB} & \eta_2^{AB} \end{bmatrix} \begin{Bmatrix} a_1^{AB} \\ a_2^{AB} \end{Bmatrix} \tag{19}$$

or $\mathbf{d}^A = \mathbf{S}^A\mathbf{a}^A$. The derivation of other boundary conditions is also straightforward.

The upper end D of the pile with a lumped mass is assumed to be semi-rigidly connected and the horizontal displacement is not restricted. Thus, we have

$$Q^{DE} = Q^{DC} + m\frac{\partial^2 v^{DC}}{\partial t^2} = 0, \quad M^{DE} = M^{DC} - J\frac{\partial^2 \phi^{DC}}{\partial t^2} \tag{20}$$

On the other hand, DE element means the semi-rigid connection. So we can obtain the following relations

$$M^{ED} = (\phi_E - \phi_D)\cdot k_\phi, \quad \phi_E = 0 \tag{21}$$

in which $k_\phi = R \cdot EI/L$. From Eqs. (20) and (21), we have

$$\mathbf{d}^D = \mathbf{S}^D\mathbf{a}^D \tag{22}$$

If a harmonic horizontal force $F = F_0 e^{i\omega t}$ or a harmonic moment $M = M_0 e^{i\omega t}$ is applied on the upper end of the pile, Eq. (23) should be $\mathbf{d}^D = \mathbf{S}^D\mathbf{a}^D + \mathbf{Q}_0$, where $\mathbf{Q}_0$ is the local force vector. Combining all equations in Eqs. (13), (18), (19) and (22), we arrive at a global scattering relation as follows

$$\mathbf{d} = \mathbf{S}\mathbf{a} + \mathbf{Q} \tag{23}$$

where $\mathbf{Q}$ is the global force vector, $\mathbf{d}$ is the global vector associated with departing waves, $\mathbf{a}$ is the global vector associated with arriving waves, and $\mathbf{S}$ is the global scattering matrix (Pao *et al.* 2007, Pao and Chen 2009). For each pile element, two different local coordinate systems have been employed. Because of the unique physical reality, solutions of the two systems should predict identical result. For example, at identical point $x^{ij} = l^{ij} - x^{ji}$ on the pile segment BC, we have

$$\bar{v}^{BC}(x^{BC}) = \bar{v}^{CB}(l^{BC} - x^{CB}) \tag{24}$$

which yields

$$\begin{aligned} a_1^{BC} e^{\beta_1^{BC} l^{BC}} &= -d_1^{CB}, \quad a_2^{BC} e^{\beta_2^{BC} l^{BC}} = -d_2^{CB} \\ d_1^{BC} e^{-\beta_1^{BC} l^{BC}} &= -a_1^{CB}, \quad d_2^{BC} d^{-\beta_2^{BC} l^{BC}} = -a_2^{CB} \end{aligned} \tag{25}$$

Eq. (25) gives relations connecting the arriving waves in one local coordinates to the departing waves in another local coordinates, and are called phase relations (Pao *et al.* 2007, Pao and Chen 2009). Introducing a new local vector $\bar{\mathbf{d}}^B$ at joint B yields

$$\bar{\mathbf{d}}^B = [d_1^{AB}, d_2^{AB}, d_1^{BC}, d_2^{BC}]^T \tag{26}$$

Hence, a new global vector $\bar{\mathbf{d}}$ for the departing waves is constructed as

$$\bar{\mathbf{d}} = [(\bar{\mathbf{d}}^A)^T \ (\bar{\mathbf{d}}^B)^T \ (\bar{\mathbf{d}}^C)^T \ (\bar{\mathbf{d}}^D)^T]^T \tag{27}$$

where $\bar{\mathbf{d}}^A = [d_1^{BA}, d_2^{BA}]^T$ and $\bar{\mathbf{d}}^D = [d_1^{CD}, d_2^{CD}]^T$. The global vectors $\bar{\mathbf{d}}$ and $\mathbf{d}$ contain the same elements but are sequenced in different orders. The two vectors thus can be related through a permutation matrix $\mathbf{U}$ of order 12 × 12 as

$$\bar{\mathbf{d}} = \mathbf{U}\mathbf{d} \tag{28}$$

where

$$\mathbf{U} = \text{diag}[\mathbf{U}^0_{4\times4} \ \mathbf{U}^0_{4\times4} \ \mathbf{U}^0_{4\times4}], \quad \mathbf{U}^0 = \begin{bmatrix} 0 & \mathbf{I}_{2\times2} \\ \mathbf{I}_{2\times2} & 0 \end{bmatrix} \tag{29}$$

where $\mathbf{I}_{2\times2}$ is unit matrix of order 2. Notice that Eq. (25) is valid for all pile segments. Thus, these relations can be combined in a matrix form as follows

$$\mathbf{a} = \mathbf{P}\bar{\mathbf{d}} \tag{30}$$

where the total phase shift matrix $\mathbf{P}$ of order 12 × 12 is defined by

$$\mathbf{P} = [\mathbf{P}^{AB} \ \mathbf{P}^{BC} \ \mathbf{P}^{CD}] \tag{31}$$

where $\mathbf{P}^{ij} = \text{diag}[e^{-\beta_1^{ij} l^{ij}} \ e^{-\beta_2^{ij} l^{ij}} \ e^{-\beta_1^{ij} l^{ij}} \ e^{-\beta_2^{ij} l^{ij}}]$. Note that the phase matrices $\mathbf{P}^{ij}$ do not contain exponential functions with large positive indices and hence the numerical instability usually encountered in the conventional transfer matrix method (TMM) (Pestel and Leckie 1963) can be avoided. This is a crucial point for the proper application of MRRM in high-frequency dynamic analysis of structures (Yan *et al.* 2007a, 2007b). From Eqs. (23), (28) and (30), we obtain

$$(\mathbf{I} - \mathbf{R})\mathbf{d} = \mathbf{Q} \tag{32}$$

where $\mathbf{R} = \mathbf{S}\mathbf{P}\mathbf{U}$ is called the reverberation-ray matrix of order 12 × 12 (Pao *et al.* 2007, Pao and Chen 2009). The following relations then hold

$$\mathbf{d} = (\mathbf{I} - \mathbf{R})^{-1}\mathbf{Q}, \quad \mathbf{a} = \mathbf{P}\mathbf{U}\mathbf{d} \tag{33}$$

Hence, all undetermined constants in Eqs. (8) and (10) can be solved from Eq. (33). If there is no external harmonic forces applied on the pile, we have $\mathbf{Q} = \mathbf{0}$. Thus, the frequency equation governing the free vibration of the pile can be obtained by letting the coefficient determinant of Eq. (32) vanish, i.e.

$$\det[\mathbf{I} - \mathbf{R}] = 0 \tag{34}$$

4. Numerical analysis

4.1 Comparison study

To validate the present analysis, the free vibration of a series of reinforced-concrete cantilever walls depicted in Fig. 2 is investigated. The material constants and geometric parameters for each specimen are listed in Table 1, as well as Poisson ratio $\mu = 0.15$; length of the wall $L = 4.57$ m; and a lump mass at the upper end with $m = 1404.51$ kg and $J = 657.93$ kgm^2 are assumed (Arboleda-Monsalve *et al.* 2008). The fundamental natural frequencies for all eight walls are calculated by the frequency Eq. (34) and are listed in Table 2. We can see that the numerical results obtained by the present method agree well with both the measured (Aristizabal-Ochoa 1983) and calculated ones (Arboleda-Monsalve *et al.* 2008) except for R2 (the denotation of the specimen), for which however the two analytical solutions match perfectly with each other.

In order to investigate the effect of rotational inertia along the members on free vibration of the walls (or piles), which is usually ignored in some related works (Catal 2002, 2006), the variation of the rotational angle ϕ with the frequency f subjected to the applied moment $M_0 e^{i\omega t}$ ($M_0 = 1$ kNm) at the upper end is shown in Fig. 3. The first three natural frequencies can be extracted directly from the curve of rotational angle in the frequency domain. It can be shown that the values of the natural frequencies obtained by the model excluding rotational inertia along the wall are larger than those

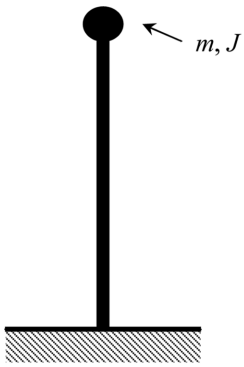

Fig. 2 Reinforced-concrete cantilever wall

Table 1 The properties of cantilever walls (Arboleda-Monsalve *et al.* 2008)

Specimen	I (m^4)	A (m^2)	$\overline{m}$ (kg/m)	κ	E (MPa)
F1	0.193	0.359	861.6	0.52	25424.1
B1	0.139	0.317	760.8	0.58	28111.2
B2	0.139	0.317	760.8	0.58	28938
B3	0.139	0.317	760.8	0.58	27284.4
B4	0.139	0.317	760.8	0.58	28249
B5	0.139	0.317	760.8	0.58	27353.3
R1	0.058	0.193	463.2	0.83	27766.7
R2	0.058	0.193	463.2	0.83	26802.1

Table 2 The first natural frequency of cantilever walls (Hz)

	Experimental results (Aristizabal-Ochoa 1983)	Numerical results (Arboleda-Monsalve *et al.* 2008)	Present method
F1	33.80	33.78	33.779
B1	30.00	32.19	32.193
B2	29.40	32.66	32.663
B3	29.70	31.72	31.718
B4	29.20	32.27	32.272
B5	30.10	31.76	31.755
R1	21.80	23.86	23.857
R2	17.80	23.44	23.440

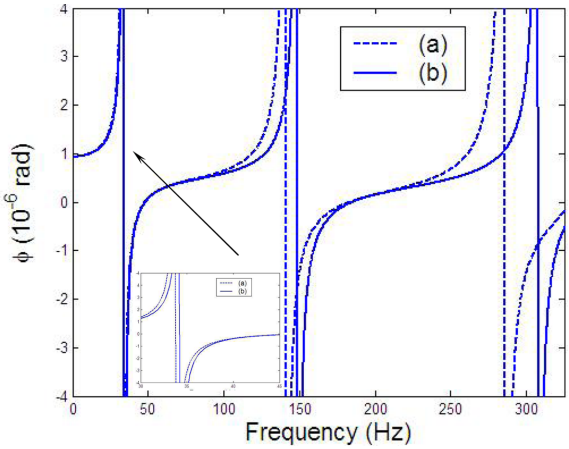

Fig. 3 Variation of rotational angle at the upper end subjected to an applied harmonic force (a) including rotational inertia along the wall, (b) excluding rotational inertia along the wall

calculated by the present method including rotational inertia along the member. The similar observations were also reported by Arboleda-Monsalve *et al.* (2008).

As mentioned before, the transfer matrix method (TMM) and the method of the dynamic stiffness matrix may encounter numerical instability in the high frequency range. To illustrate this issue, the mechanical impedance Z_s defined by Bamnios (2002) at the upper end under harmonic mechanical force is employed to reflect the dynamics of a cantilever beam. In this case, the material constants and geometric parameters are assumed to be (Guo and Chen 2007): Young's modulus $E = 3.25 \times 10^{10}$ N/m^2, mass density $\rho = 2500$ kg/m^3, shear modulus $G = 13.54 \times 10^9$ N/m^2, shear coefficient $\kappa = 0.8434$, beam length 40 m, and area of cross section $A = 13.6$ m^2. A thick beam with moment of inertia $I = 8.1592$ m^4 and a slender beam with moment of inertia $I = 4.1592$ m^4 are also assumed in this case. A comparison between MRRM and TMM for thick beam is conducted, as shown in Fig. 4(a). It can be seen that the two methods agree with each other very well. However, for the slender beam, when the frequency becomes higher, numerical instability appears in TMM while MRRM still behaves quite well, as depicted in Fig. 4(b). According to Pestel and Leckie (1963), the numerical instability appearing in TMM is caused mainly by the subtracting of two nearly equal

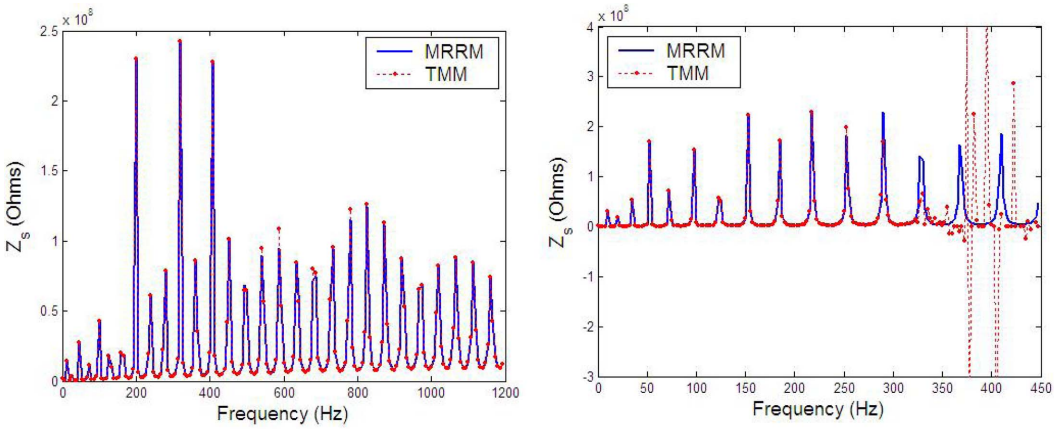

Fig. 4 Comparison study with TMM

large numbers or by a factor that grows exponentially with a parameter. For this case of Timoshenko beam, the wave number β_2 in Eq. (9) may be real when the beam becomes more slender, and the transfer matrix will contain the factor $e^{+\beta_2 l}$, which exponentially grows with the product of wave number β_2 and beam length l of the structure. However, in MRRM, the phase matrices $\mathbf{P}^{ij}$ only contain exponential functions with negative indices as shown in Eq. (31) and hence the numerical instability usually encountered in TMM can be avoided. This is the specific merit of MRRM for dynamic analysis of a structure, especially at high frequencies.

4.2 Free vibration analysis

Then, a partially embedded pile with a semi-rigid connection at the upper end is studied. The physical parameters of the reinforced-concrete pile are listed in Table 3 and meanwhile the length of

Table 3 The parameters of the reinforced-concrete pile (Arboleda-Monsalve *et al.* 2008)

Cross section (m^2)	k_s (N/m^2)	k_G^0 (N)	$\overline{m}$ (kg/m)	κ	G (MPa)	E (MPa)
0.50 × 0.50	2068400	3200000	600	0.83	11307.40	25998.75

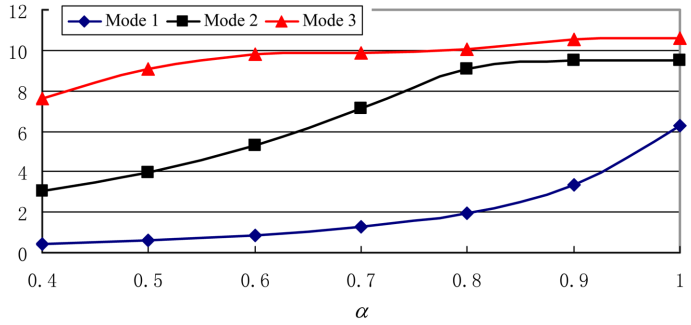

Fig. 5 Effect of α on the natural frequencies of the pile ($f_R = 0.6$, $N_r = 0.6$, $c = 0$)

pile 30 m, and the lumped mass at the upper end with $m = 2000$ kg and $J = 800$ kgm^2 are assumed. We define the following quantity in this paper

$$\alpha = \frac{L_2}{L}, \quad \beta = \frac{k_G}{k_G^0}, \quad N_r = \frac{NL^2}{\pi^2 EI}, \quad f_R = \frac{R}{3+R} \tag{35}$$

where the transverse modulus k_G^0 is listed in Table 3, β always equals to 1 unless otherwise stated.

Fig. 5 shows the effect of the ratio of the embedded length to the total length of the pile α on the first three natural frequencies in the case of $f_R = 0.6$, $N_r = 0.6$, and $c = 0$. It can be seen that all

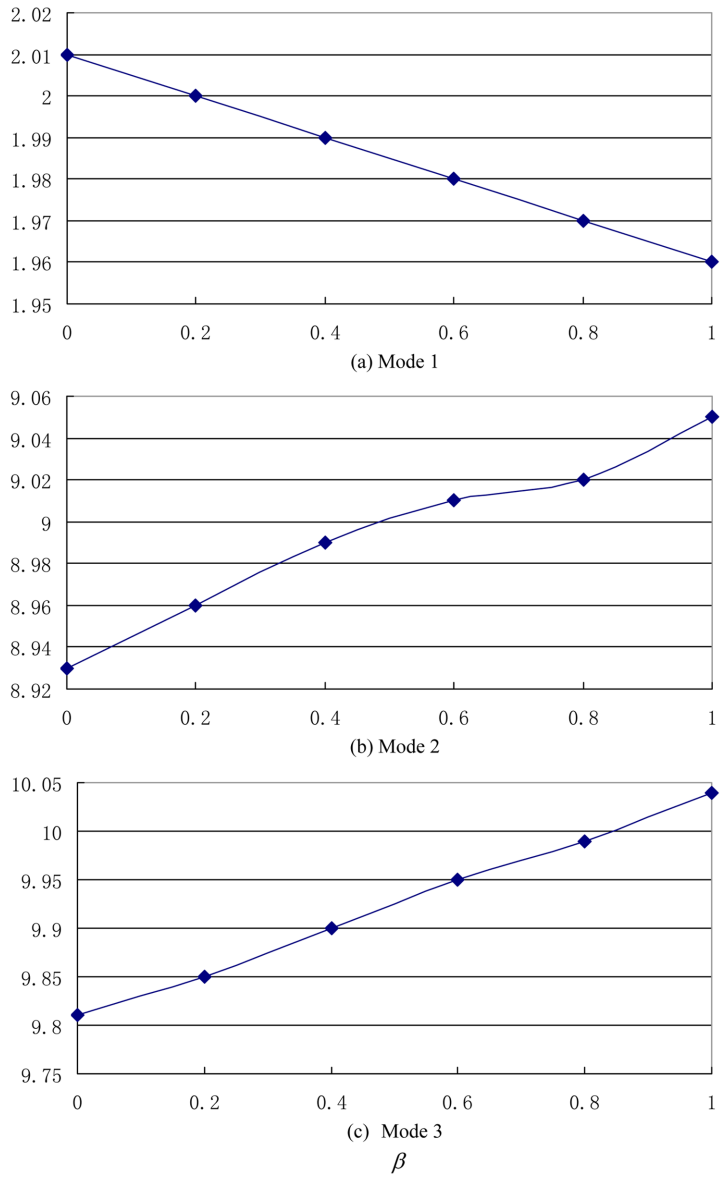

Fig. 6 Effect of β on the natural frequencies of the pile ($f_R = 0.6$, $N_r = 0.6$, $c = 0$, $\alpha = 0.8$)

three mode frequencies, especially the fundamental natural frequency, increase significantly with α from 0.4 to 1. When β approaches zero, i.e., the transverse modulus k_G = 0, the proposed two-parameter elastic foundation model (Arboleda-Monsalve *et al.* 2008, Celep *et al.* 2011) will degenerate to the Winkler model, in which the effect of shear foundation modulus through the pile length is neglected (Catal 2006). We can observe from Fig. 6 that the transverse modulus k_G influences the first three mode frequencies slightly and the difference between the calculated results by both the elastic foundation models is less than 2.5 percent. From Fig. 7, we can see that all three mode frequencies decrease clearly with N_r from 0 to 1. Fig. 8 shows that the fixity factor has an

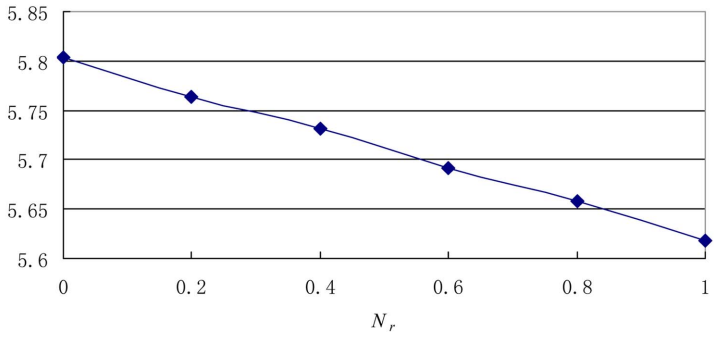

(a) Mode 1

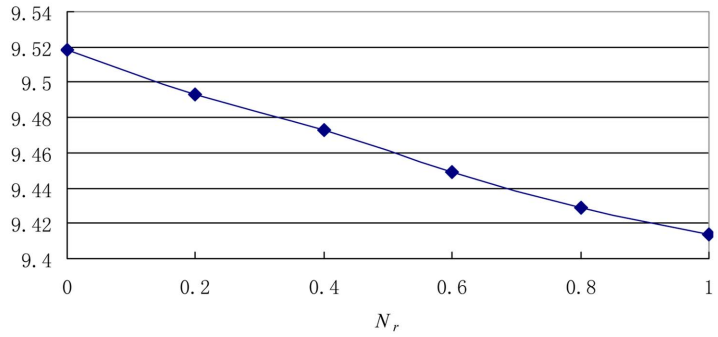

(b) Mode 2

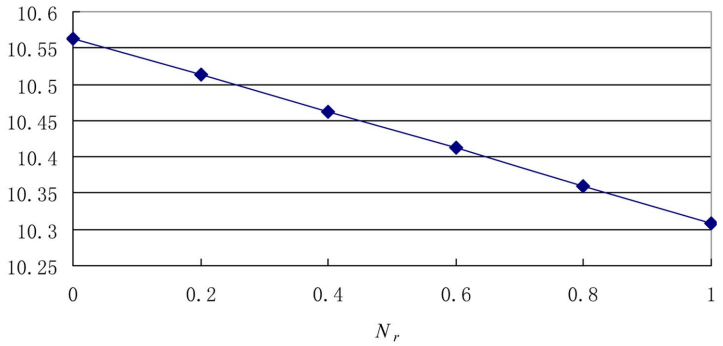

(c) Mode 3

Fig. 7 Effect of axial force on the natural frequencies of the pile ($\alpha = 1$, $f_R = 0$, $c = 0$)

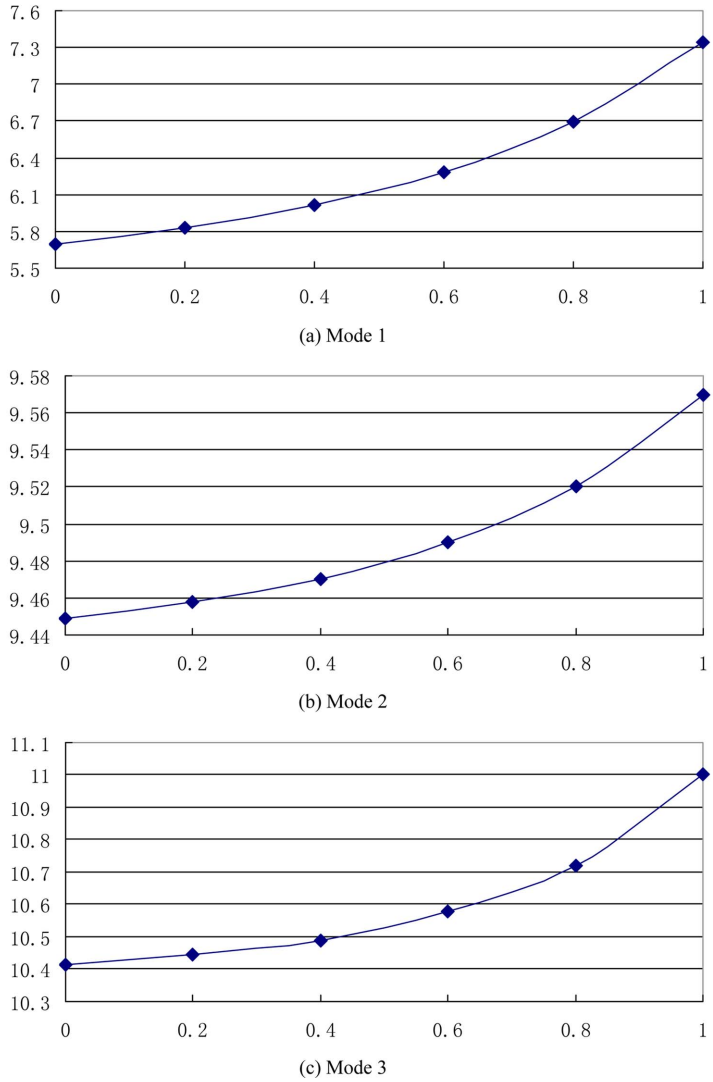

Fig. 8 Effect of fixity factor f_R on the natural frequencies of the pile ($\alpha = 1$, $N_r = 0.6$, $c = 0$)

evident effect on the free vibration characteristic of the pile. However, a crack appearing in the middle of the pile can hardly change the first three frequencies, even for a deep crack with $c = 0.30$ m, as shown in Fig. 9.

4.3 Frequency response analysis

In this paper, the frequency response function (FRF) data is defined as the ratio of the applied force to the transverse velocity of the applied point, i.e., the mechanical impedance Z_s (Bamnios 2002). Since the expression for complex frequency response such as $\overline{v}(\omega)$ contains departing and arriving wave amplitudes determined from Eq. (33), for undamped structures, it has an infinite number of poles along the real ω axis which corresponds to the natural frequencies predicted by Eq.

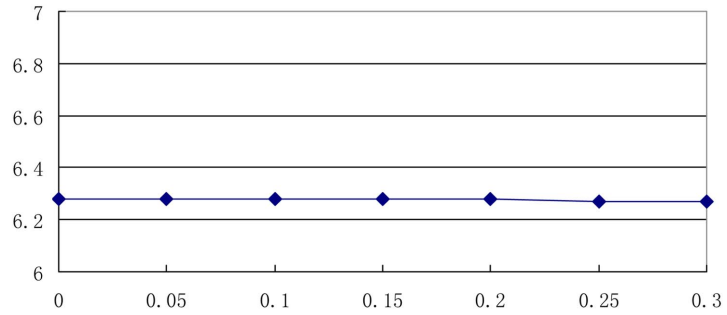

(a) Mode 1

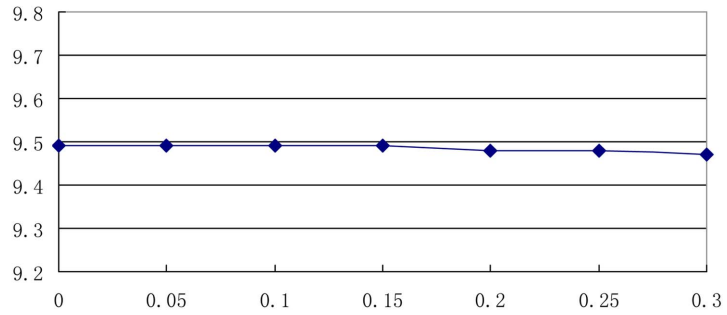

(b) Mode 2

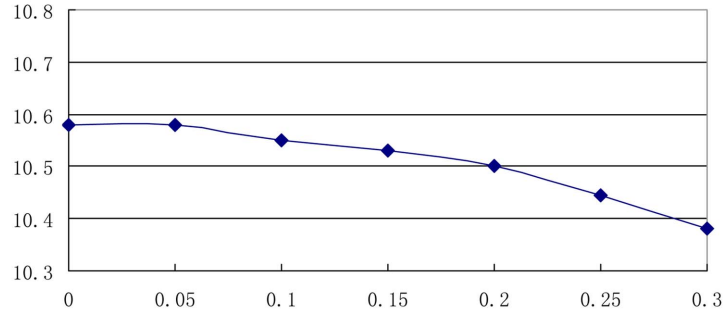

(c) Mode 3

c (m)

Fig. 9 Effect of crack depth on the natural frequencies of the pile ($\alpha = 1$, $f_R = 0.6$, $N_r = 0.6$)

(34) based on the direct inverse of $(\mathbf{I}-\mathbf{R})$ and thus inaccurate results near these poles will be obtained due to the singular behavior (Guo and Chen 2007, Guo *et al.* 2008, Jiang and Chen 2009). In order to avoid the singularities encountered in the numerical computations, the Neumann series expansion technique (Pao *et al.* 2007, Pao and Chen 2009, Jiang and Chen 2009) is usually employed and $(\mathbf{I}-\mathbf{R})^{-1}$ in Eq. (33) can be expanded as follows

$$(\mathbf{I}-\mathbf{R})^{-1} = \mathbf{I}+\mathbf{R}+\mathbf{R}^2+\ldots+\mathbf{R}^N+\ldots \tag{36}$$

However, using different terms N in the Neumann series usually gives quite different results, further indicating that the Neumann series expansion technique is inapplicable to the frequency response analysis (Guo and Chen 2007). To overcome this difficulty, the artificial damping technique (Guo and Chen 2007, Guo *et al.* 2008) by adding appropriate small damping into the structural system is employed here. It is actually more physically realistic, because damping always exists in a real structure. Thus, in the following computation, the damping ratio is always taken to be 0.02.

We can observe from Figs. 10-12 that the ratio of the embedded length to the total length of the pile α, the ratio of the applied axial load to the Euler buckling load N_r, and the fixity factor f_R have evident effect on the dynamic properties of the pile and hence significantly alter the steady-state response of the structural system. For example, a decrease in the connection fixity factor reduces the

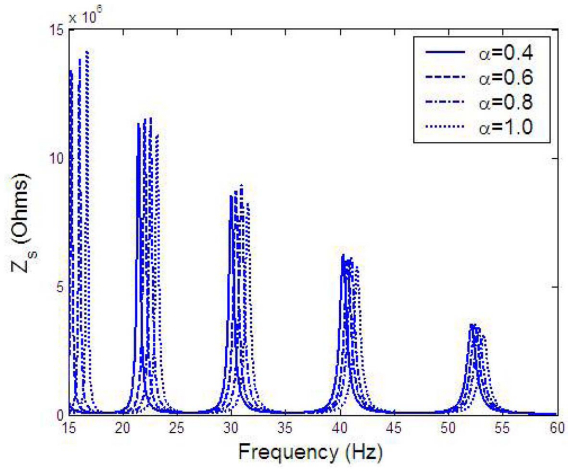

Fig. 10 Effect of α on the frequency response of the pile ($f_R = 0.6$, $N_r = 0.6$, $c = 0$)

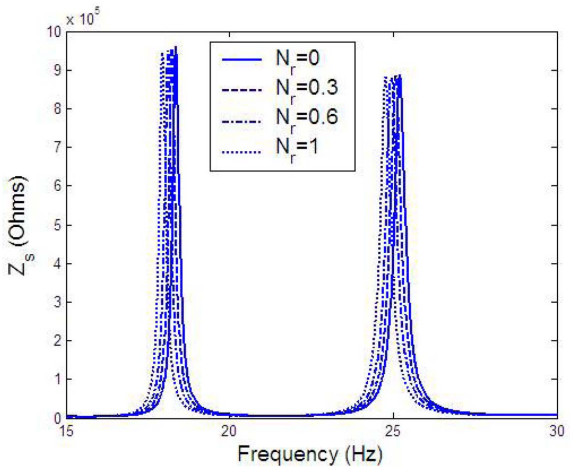

Fig. 11 Effect of axial forces on the frequency response of the pile ($\alpha = 1$, $f_R = 0.6$, $c = 0$)

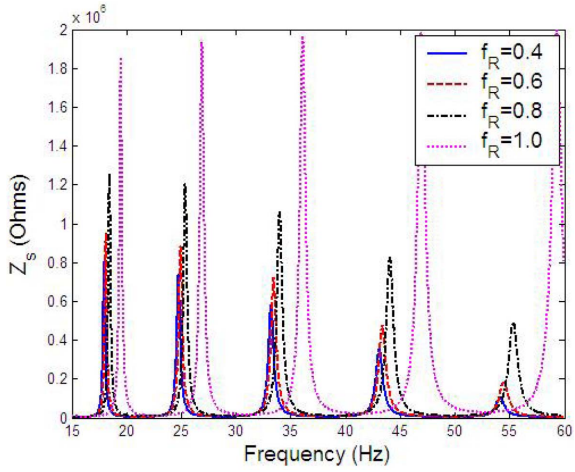

Fig. 12 Effect of fixity factor f_R on the frequency response of the pile ($\alpha = 1$, $N_r = 0.6$, $c = 0$)

pile stiffness, and thus the peaks of mechanical impedance Z_s shift leftwards clearly as predicted by MRRM (see Fig. 12). This indicates that the resonant frequencies decrease for a pile with increasing connection flexibility. This observation agrees well with the numerical results for free vibration depicted in Fig. 8. The similar observations for the influence of parameters α and N_r on frequency responses are also obtained as shown in Figs. 10-11.

A frequency-domain method is considered to be an effective structural damage identification technique (Lee and Shin 2002), in which only the frequency response function (FRF) data are required. Although a crack appearing in the pile can hardly change the first three frequencies as depicted in Fig. 9, we can see from Fig. 13 that it can yield significant deviation of decades of Hz in the high frequency range by the mechanical impedance-based method (Bamnios 2002). This indicates that the high-frequency signatures are more sensitive to incipient cracks in piles. The effect of crack positions on steady-state response of the piles is further illustrated in Fig. 14, in which S denotes the distance between the crack position and the bottom end of the pile.

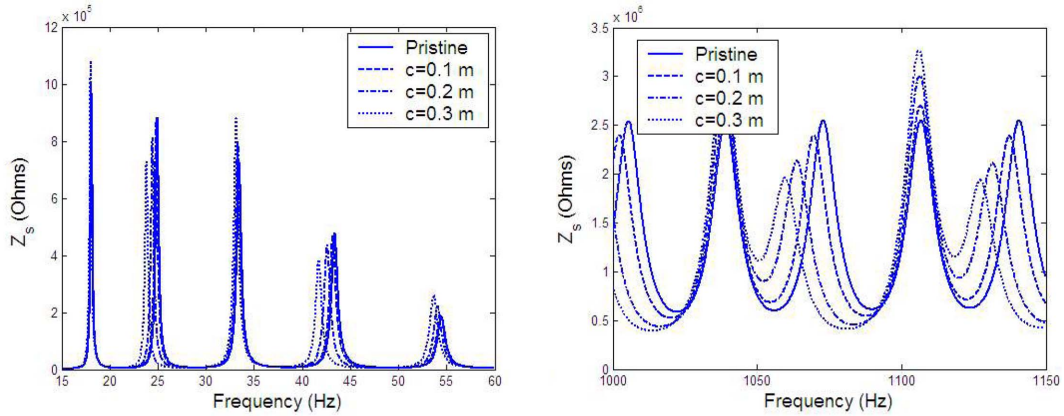

Fig. 13 Effect of crack depth on the frequency response of the pile ($\alpha = 1$, $f_R = 0.6$, $N_r = 0.6$)

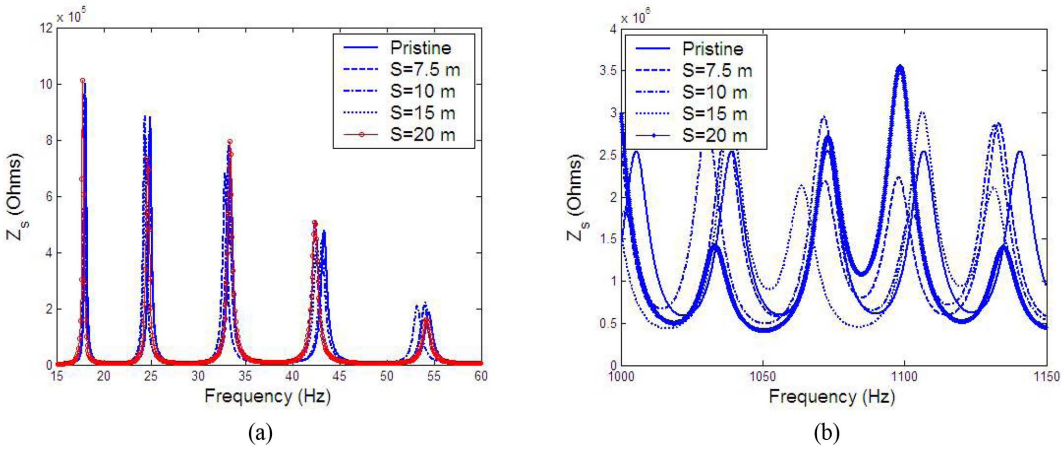

Fig. 14 Effect of crack location on the frequency response of the pile ($\alpha = 1$, $f_R = 0.6$, $N_r = 0.6$, $c = 0.2$ m)

4.4 Transient response analysis

The transient response, such as the transverse displacement $v(x,t)$ at the upper end of the pile, can be obtained by the inverse Fourier transform (IFT) of the frequency response as

$$v(x,t) = \frac{1}{2\pi}\int_{-\infty}^{\infty} \bar{v}(x,\omega)e^{i\omega t}d\omega \tag{37}$$

In Fast Fourier Transform algorithm, a longer time period should be used to reduce the aliasing error due to the dispersive flexural waves and meanwhile the time interval should be kept small to meet the requirement of cut-off frequency. Thus, the Neumann series expansion technique is also unsuitable for the calculation of medium and long time transient responses due to its low calculation efficiency (Guo and Chen 2007) and the artificial damping technique is sequentially employed in the transient response analysis.

Now consider that a dynamic load of a rectangular pulse is applied on the point of ground surface, i.e., node *C*, as shown in Fig. 1.

$$F(t) = \begin{cases} 10^5 \text{ N} & 0 \le t \le 0.3 \text{ s} \\ 0 \text{ N} & t > 0.3 \text{ s} \end{cases} \tag{38}$$

The transverse displacements v at the upper end of the pile calculated in the time domain are presented in Figs. 15-19 for period of duration 1.2 s with a time step 0.004 s. It should be noted that because the fundamental natural frequency of the pile with small parameter α is very low (see Fig. 5), a larger period of duration is necessary for investigating the influence of the physical parameter α on transient response.

It can be seen from Fig. 15 that the motion periods of the piles becomes shorter evidently with increasing parameter α. This observation agrees well with those plotted in Figs. 5 and 10 for free vibration and steady-state responses, respectively. The time histories of the transverse displacements at the upper end of the pile with various axial forces, fixity factors, crack depths and locations are plotted in Figs. 16-19, respectively. A visible increase of the displacement amplitudes and a slight

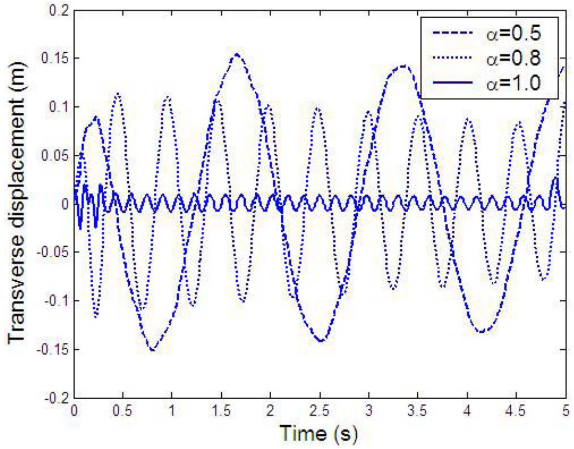

Fig. 15 Effect of α on the transient response of the pile ($f_R = 0.6$, $N_r = 0.6$, $c = 0$)

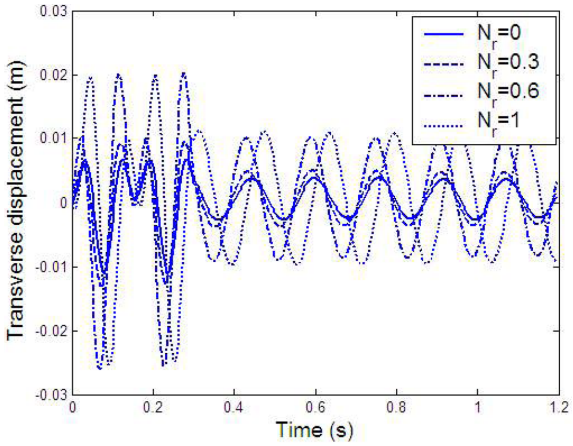

Fig. 16 Effect of axial forces on the transient response of the pile ($\alpha = 1$, $f_R = 0.6$, $c = 0$)

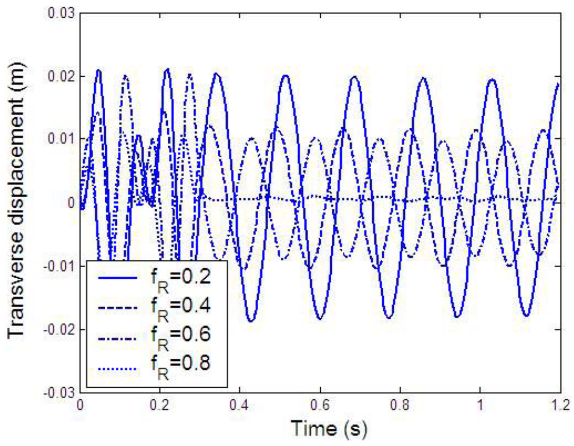

Fig. 17 Effect of fixity factor f_R on the transient response of the pile ($\alpha = 1$, $N_r = 0.6$, $c = 0$)

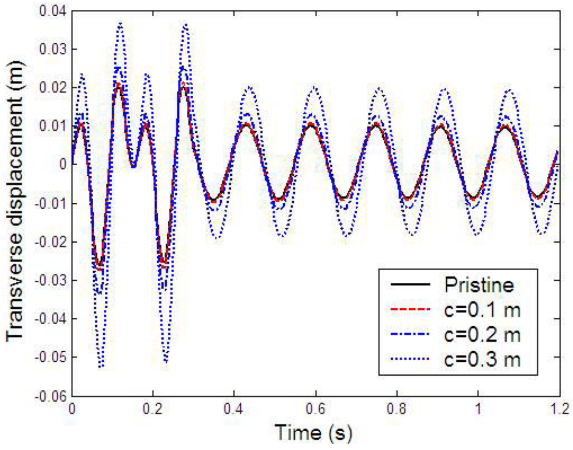

Fig. 18 Effect of crack depth on the transient response of the pile ($\alpha = 1$, $f_R = 0.6$, $N_r = 0.6$)

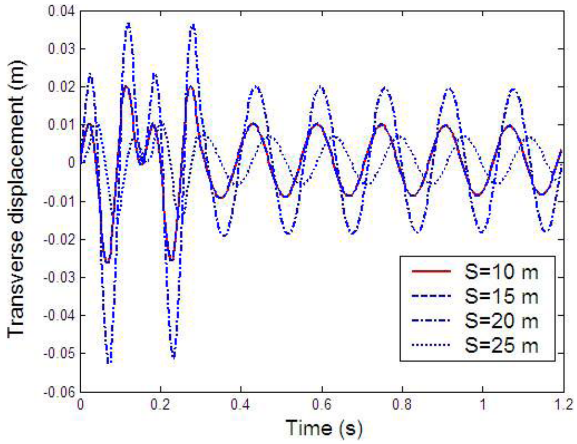

Fig. 19 Effect of crack location on the transient response of the pile ($\alpha = 1$, $f_R = 0.6$, $N_r = 0.6$, $c = 0.2$ m)

increase of motion periods can be observed from Fig. 16 with the increasing axial forces. Contrarily, with the increasing fixity factors, the displacement amplitudes and motion periods have evident decreases as shown in Fig. 17. Cracks appearing in the piles seem to have little influence on the motion period even for a deep crack with $c = 0.3$ m (see Fig. 18). However, various crack locations may result in the obvious change of transient responses especially for a closer crack to the upper end of the pile, as shown in Fig. 19.

5. Conclusions

Piles partially embedded in two-parameter elastic foundations and flexibly connected with the substructures are investigated by the method of reverberation-ray matrix. The model employs Timoshenko beam theory with the cracks in the piles treated as massless rotational springs.

Comparison with existent numerical and experimental results indicates that the proposed technique is very effective and accurate for dynamic analysis even in the high frequency range.

Numerical results show that the dynamic properties of the piles are highly sensitive to some physical parameters such as the ratio of the embedded length to the total length of the piles and the fixity factor of the semi-rigid joints. This indicates that the connections between the piles and the superstructures play very important roles for the behavior and safety of the structures subjected to strong dynamic loads. The applied axial force at the upper end also has a clear effect on the free vibration, frequency response and transient response of the piles. The dynamic properties of the piles seems insensitive to the transverse modulus k_G. This indicates that a Winkler model adopted in some works (Catal 2002, 2006) is accurate enough to simulate the behavior of elastic soil in the field of engineering. A single crack initiating in a pile, even with a profound depth, can hardly change the global stiffness of the pile and consequently it has little effect on the free vibration of the piles in the low frequency range. Contrarily, the high-frequency mechanical impedance data is very sensitive to the crack. This indicates that a high frequency domain method is more appropriate to detect minor cracks in the piles or beams.

Acknowledgements

The work was sponsored by the National Natural Science Foundation of China (Grant No. 10725210), the National Basic Research Program of China (No. 2009CB623204), the program of Key Team of Technological Innovation of Zhejiang Province (Grant No. 2011R09025-03) and K.C. Wong Magna Fund in Ningbo University.

References

Allotey, N., and EI Naggar, M.H. (2008), "A numerical study into lateral cyclic nonlinear soil-pile response", *Can. Geotech. J.*, **45**, 1268-1281.

Arboleda-Monsalve, L.G., Zapata-Medina, D.G. and Aristizabai-Ochoa, J.D. (2008), "Timoshenko beam-column with generalized end conditions on elastic foundation: Dynamic-stiffness matrix and load vector", *J. Sound Vib.*, **310**, 1057-1079.

Aristizabal-Ochoa, J.D. (1983), "Cracking and shear effects on structural walls", *J. Struct. Eng.-ASCE*, **109**(5), 1267-1277.

Bamnios, Y. (2002), "Crack identification in beam structures using mechanical impedance", *J. Sound Vib.*, **256**(2), 287-297.

Bhalla, S., and Soh, C.K. (2004), "High frequency piezoelectric signatures for diagnosis of seismic/blast induced structural damages", *NDT & E Int.*, **37**, 23-33.

Catal, H.H. (2002), "Free vibration of partially supported piles with the effects of bending moment, axial and shear force", *Eng. Struct.*, **24**, 1615-1622.

Catal, H.H. (2006), "Free vibration of semi-rigid connected and partially embedded piles with the effects of the bending moment, axial and shear force", *Eng. Struct.*, **28**, 1911-1918.

Catal, S. and Catal, H.H. (2006), "Buckling analysis of partially embedded pile in elastic soil using differential transform method", *Struct. Eng. Mech.*, **24**(2), 247-268.

Celep, Z., Guler, K. and Demir F. (2011), "Response of a completely free beam on a tensionless Pasternak foundation subjected to dynamic load", *Struct. Eng. Mech.*, **37**, 61-77.

Faella, C., Martinelli, E. and Nigro, E. (2008), "Analysis of steel-concrete composite PR-frames in partial shear interaction: A numerical model and some applications", *Eng. Struct.*, **30**, 1178-1186.

Guo, Y.Q. and Chen, W.Q. (2007), "Dynamic analysis of space structures with multiple tuned mass dampers", *Eng. Struct.*, **29**, 3390-3403.
Guo, Y.Q., Chen, W.Q. and Pao, Y.H. (2008), "Dynamic analysis of space frames: The method of reverberation-ray matrix and the orthogonality of normal modes", *J. Sound Vib.*, **317**, 716-738.
Jiang, J.Q. and Chen, W.Q. (2009), "Reverberation-ray analysis of moving or distributive loads on a non-uniform elastic bar", *J. Sound Vib.*, **319**, 320-334.
Lee, U. and Shin, J.A. (2002), "Frequency-domain method of structural damage identification formulated from the dynamic stiffness equation of motion", *J. Sound Vib.*, **257**, 615-634.
Lin, H.P. (2004), "Direct and inverse methods on free vibration analysis of simply supported beams with a crack", *Eng. Struct.*, **26**, 427-436.
Lu, J.F., Jeng, D.S. and Nie, W.D. (2006), "Dynamic response of a pile embedded in a porous medium subjected to plane SH waves", *Comput. Geotech.*, **33**, 404-418.
Morikawa, S.R.K., Gama, A.L., Braga, A.M.B. and Correia, R.R. (2005), "Monitoring surface breaking defects with piezoelectric active systems", *Exper. Mech.*, **45**(1), 89-95.
Nagem, R.J. and Williams, J.H. (1989), "Dynamic analysis of large space structures using transfer matrices and joint coupling matrices", *Mech. Struct. Mach.*, **17**, 349-371.
Pao, Y.H. and Chen, W.Q. (2009), "Elastodynamic theory of framed structures and reverberation-ray matrix analysis", *Acta Mechanica*, **204**, 61-79.
Pao, Y.H., Chen, W.Q. and Su, X.Y. (2007), "The reverberation-ray matrix and transfer matrix analyses of unidirectional wave motion", *Wave Motion*, **44**, 419-438.
Pestel, E.C. and Leckie, F.A. (1963), *Matrix Methods in Elasto Mechanics*, McGraw-Hill, New York.
Rajasekaran, S. (2008), "Buckling of fully and partially embedded non-prismatic columns using differential quadrature and differential transformation methods", *Struct. Eng. Mech.*, **28**, 221-238.
Sekulovic, M., Salatic, R. and Nefovska, M. (2002), "Dynamic analysis of steel frames with flexible connections", *Comput. Struct.*, **80**, 935-955.
Timoshenko, S.P. and Gere, J.M. (1961), *Theory of Elastic Stability, Engineering Societies Monographs*, McGraw-Hill Book Company, New York.
Yan, W., Chen, W.Q., Lim, C.W. and Cai, J.B. (2008), "Application of EMI technique for crack detection in continuous beams adhesively bonded with multiple piezoelectric patches", *Mech. Adv. Mater. Struct.*, **15**, 1-11.
Yan, W., Lim, C.W., Chen, W.Q. and Cai, J.B. (2007a), "A coupled approach for damage detection of framed structures using piezoelectric signature", *J. Sound Vib.*, **307**, 802-817.
Yan, W., Lim, C.W., Chen, W.Q. and Cai, J.B. (2007b), "Modeling of EMI response of damaged Mindlin-Herrmann rod", *Int. J. Mech. Sci.*, **49**, 1355-1365.
Yesilce, Y. and Catal, H.H. (2008a), "Free vibration of piles embedded in soil having different modulus of subgrade reaction", *Appl. Math. Model.*, **32**(5), 889-900.
Yesilce, Y. and Catal, H.H. (2008b), "Free vibration of semi-rigid connected Reddy-Bickford piles embedded in elastic soil", *Sadhana-Academy Prooceedings in Engineering Sciences*, **33**(6), 781-801.
Yesilce, Y. and Catal, H.H. (2008c), "Free vibration of semi-rigidly connected piles embedded in soils with different subgrades", *Int. J. Struct. Stab. D.*, **8**(2), 299-320.

Notations

$\mathbf{a}$: global vector associated with arriving waves
c : the depth of the crack
$\mathbf{d}$: global vector associated with departing waves
f : frequency
f_R : fixity factor
h : thickness of the pile
i : $\sqrt{-1}$
k_s, k_G : the ballast modulus and the transverse modulus for the two-parameter elastic foundation model, respectively
m : a lumped mass attached at the extreme D
v : displacement component in the y direction
x, y : Cartesian coordinates
A : cross sectional area of the pile
E : Young's modulus of the pile
G : shear rigidity of the pile
I : moment of inertia of the pile
J : rotational moment of inertia of the pile
L : length of the pile
M, Q : bending moment and shear force, respectively
$\mathbf{Q}$: global force vector
N : constant force along the centroidal axis
N_r : ratio of the applied axial load to the Euler buckling load
$\mathbf{P}$: total phase shift matrix
$\mathbf{R}$: reverberation-ray matrix
R : bending stiffness index of the flexural connections
$\mathbf{S}$: global scattering matrix
$\mathbf{U}$: permutation matrix
Z_s : mechanical impedance
α : ratio of the embedded length to the total length of the pile
ϕ : rotation
γ : non-dimensional crack-depth ratio
η : mechanical loss factors
κ : shear correction factor ($\kappa = 10(1+\mu)/(12+11\mu)$ (Lin 2004)
μ : Poisson's ratio of the pile
ρ : mass density of the pile
ω : circular frequency